THE EXPERIENCE OF HIGH PRESSURE RATIO SINGLE STAGE HPT DESIGNING

V.D. Venediktov*, V.G Krupa*, S.V. Rudenko*, A.D. Nepomnyashchiy*,
V.K. Sichev, A.A. Shvirev****
CIAM, *«Aviadvigatel»**
nepomnashi@ciam.ru

Key words: *experimental module, high-pressure turbine, intermediate duct*

Abstract

Some results of calculated and experimental investigations of the high loading single-stage cooled high-pressure turbine (HPT) for a turbofan engine of the civil aviation are shown in this paper. Some results of calculated investigation of the intermediate duct (ID) located between the investigated HPT and the multi-stage low pressure turbine (LPT) are also shown in this paper. Investigations of the HPT were conducted within the experimental module, which includes HPT + ID + first-stage nozzle block of the LPT + guide vane (GV) with the heated air at its inlet.

1 Introduction

Improving the fuel efficiency of turbofan engines of the civil aviation obtains by increasing the engine's bypass ratio and the total degree of engine's pressure ratio. This trend leads to an increase of the pressure ratio in an HPT up to levels of 4.5-5.5. This pressure ratio may be realized in a two-stage HPT or in a single stage HPT.

The main advantage of a single-stage HPT is reduction of its length almost in 2 times and the number of its parts, as well as the decrease in the amount of cooling air in comparison with their values in an two-stage HPT. In addition, a single-stage HPT is located at a larger diameter, which reduces the radial dimensions of the ID between an HPT and an LPT and makes it less aggressive.

The main disadvantage of a single-stage HPT is a low value of efficiency, as well as more severe heat-stressed conditions of its operation compared with the operation's conditions of a two-stage HPT. Due to strength limitations, speed coefficient u/c_{is} (this coefficient is equal to a loading factor; c_{is} – isentropic velocity, u – rotation speed at the mid diameter of the turbine blade) of a single-stage HPT does not exceed the values of 0.43-0.45, which reduces efficiency and leads toward an appearance of a significant flow swirl at an HPT's outlet. A flow swirl behind an HPT can be used effectively in the case of counter rotating rotors of a turbofan engine.

Since 2004 the CIAM have been holding in conjunction with the Aviadvigatel calculated investigations aimed at the design and development of the high loading (π_{HPT}^{*} = 4.5-5.0) single-stage cooled HPT for a turbofan engine of the civil aviation. In 2009 the CIAM were conducted experimental studies of the full-sized high loaded HPT designed and manufactured at the Aviadvigatel.

Similar investigations were carried out in the DLR and the Rolls-Royce. In particular, in [1] results of the calculated and experimental investigation of the single-stage high loaded HPT (power of 1.2 MW, which was designed at the stage pressure ratio of 4.0-4.5) are shown. The experimental module was made by the scheme HPT + ID, the presence of the first-stage nozzle block of the LPT in the experimental module was not provided. Therefore, the experimental investigation did not take into account the inverse effect of the nozzle block of the LPT on a flow through the ID.

Results of the experimental investigation of the single-stage HPT within the experimental module, which includes HPT + ID + first-stage

nozzle block of the LPT are presented in [2]. The Power of the HPT was 1.59 MW at the stage pressure ratio of 3.1. The main attention in [2] is paid to investigation of the ID. The output to input area ratio of the ID was 1.5; the ratio of ID's length to HPT's blade height was 2. Total pressure losses in the ID was ~ 3%.

2 Experimental module

The scheme of the experimental module is shown in Fig. 1.

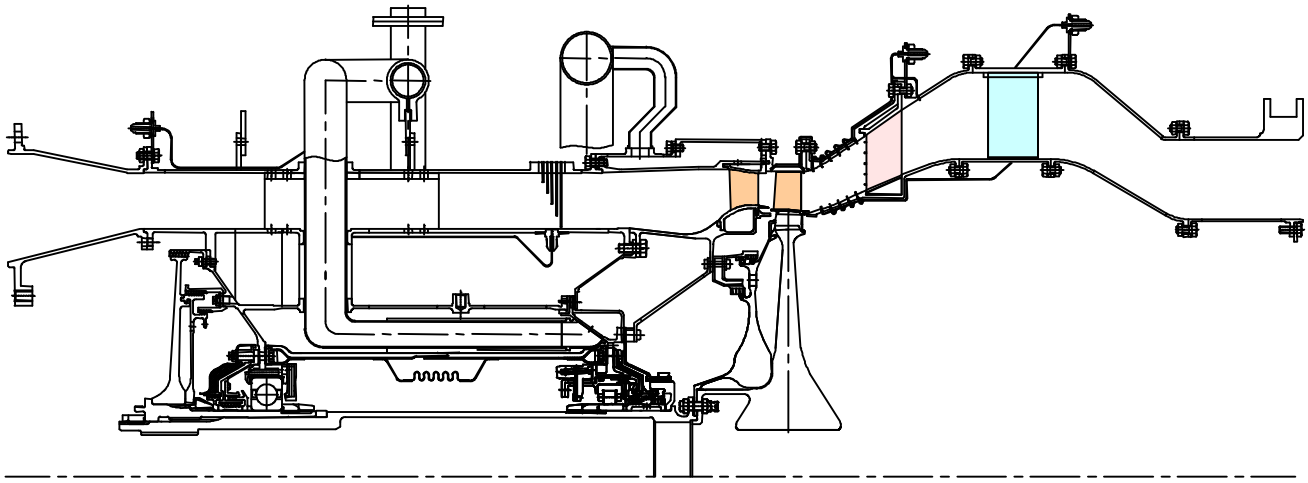

Fig. 1. The scheme of the experimental module for the investigation of the high loaded single-stage HPT with the ID and the first-stage nozzle block of the LPT.

The main gas-dynamic parameters of the HPT in a model cruise conditions are shown in Table 1. These parameters were obtained from pass-through 3D RANS calculation of the whole experimental module. The calculation was performed taking into account the issues of cooling air into a flow part of the HPT, the magnitude of the radial clearance of the rotor blades was assumed equal to 0.45 mm.

Tests were conducted at a total air temperature of 550 K at the inlet of the experimental module, and the stage pressure ratio of 4.6.

As can be seen in Table 1 the HPT was designed with high reactivity degree, which varies from the hub to the shroud within the range of 0.42-0.54. The increased reactivity degree leads to an improvement of a flow field inside blades channels of the HPT, helping to reduce losses. However, the flow swirl behind the HPT increases significantly. In particular, at the mid diameter the swirl angle at the HPT's exit was 51.1 degree. The nozzle vanes of the HPT were leant toward the direction of rotor rotation of about 7.5 degree from the radial direction. This led to a displacement of a mass flow toward the hub and decrease the flow swirl behind the nozzle vane near the end wall at the hub.

Table 1 The main gas-dynamic parameters of the HPT

		Dimension	Section		
			hub	mid	shroud
Flow angles	α_1	degree	16.4	12.3	8.4
	β_2	degree	21.1	18.9	29.3
Reactivity degree	ρ_T	–	0.42	0.48	0.54
Velocities	M_{c1}	–	1.07	1.08	0.91
	M_{w2}	–	1.14	1.26	1.19
	M_{c2}	–	0.50	0.54	0.63
	α_2	degree	56.8	51.1	79.1
Blade's diameter at the exit	D_{blade}	mm	606.0	651.0	696.0
Inlet temperature	T_0^*	K	550		
Stage pressure ratio	π_{HPT}^*	–	4.6		
Speed coefficient	u/c_{is}	–	0.47		

3 Instrumentation and measurement locations

At the HPT's inlet the total pressure was measured by means of four rakes at five points along the radius of a flow part and the total temperature was measured by means of three

rakes of thermocouples at five points along the radius. In addition, the static pressure was measured at the hub and at the shroud of a flow part at four points around the circumference. In the axial gap of the HPT the static pressure was measured at the hub and at the shroud of a flow part at three points around the circumference.

At the exit of the HPT the total pressure was measured by means of two rakes at seven points along the radius of a flow part and the total temperature was measured by means of the two rakes of thermocouples at four points along the radius. In addition, the static pressure was measured at the hub and at the shroud of a flow part at three points around the circumference.

The rotor speed and the torque of the hydraulic brake were measured simultaneously.

Measurement errors were as follows: for the pressure - 0.25%, for the temperature - 0.2%, for the torque - 0.5%, for the rotor speed - 0.1%, for the main mass flow of the air at the HPT's inlet - 0.3%.

Error in evaluations of the HPT's efficiency was - 0.7%.

On the leading edges of the three vanes of the LPT's first-stage nozzle block the total pressure was measured by means of Pitot tubes at five points along the radius, as well as the static pressure was measured at the hub and at the shroud at three points around the circumference. At the output of the nozzle block of the LPT the static pressure was measured at the hub and at the shroud of a flow part at three points around the circumference.

The main mass flow of the air entering to the HPT's inlet was measured by means of the calibrated cooled metering nozzle. The mass flow the of cooling air for the HPT's vanes and blades was measured by means of usual noncooled metering nozzles.

4 Results and discussion

The main experimental performances of the HPT's efficiency with a variation of the speed coefficient u/c_{is} and a different amount of the cooling air through the HPT's vanes and blades obtained at the regime with the stage pressure ratio of 4.6 are shown in Fig. 2.

The HPT's efficiency of the turbine was calculated using the following formula:

$$\eta^* = \frac{N}{G_0 \cdot H_0^* + G_{\text{cool.V}} \cdot H_{\text{cool}}^*} \qquad (1)$$

where N - the HPT's power measured by the hydraulic brake;

G_0 - the main mass flow of the air entering to the HPT's inlet;

$G_{\text{cool.V}}$ - the mass flow of the cooling air for the HPT's vanes issued into a flow part before nozzle throat;

H_0^* - the isentropic heat drop of the main flow of the HPT,

$$H_0^* = \frac{k}{k\text{-}1} \cdot R \cdot T_0^* \cdot (1 - \pi_{\text{HPT}}^{*\,\frac{1-k}{k}}) \qquad (2)$$

H_{cool}^* - the isentropic heat drop of the cooling air in the HPT;

$$H_{\text{cool}}^* = \frac{k}{k\text{-}1} \cdot R \cdot T_{\text{cool}}^* \cdot (1 - \pi_{\text{HPT}}^{*\,\frac{1-k}{k}}) \qquad (3)$$

It can be noticed in Fig. 2 that the value of HPT's efficiency at the model condition close to the design point ($\pi_{\text{HPT}}^* \approx 4.6$; $u/c_{is} = 0.47$ - 0.48) is 0.875.

This value of the HPT's efficiency was obtained with the high magnitude of a rotor tip clearance of 0.85 mm (instead of 0.45 mm as designed) and with a low turbulence level at the HPT's inlet. In the case of the designed radial clearance the increase of the efficiency could be about 0.015, and the HPT's efficiency at the model conditions could be 0.89.

However, under the engine operating conditions due to the high turbulence level at the HPT's inlet the decrease of the efficiency could be about 0.01. Thus, under the real engine operating conditions the HPT's efficiency could be 0.88.

Beside the main experimental performances of the HPT's efficiency there is the calculated performance of the HPT's efficiency shown in Fig. 2. It can be noticed that the calculated results predicted by CFD is in good agreement with the experimental data. This coincidence could be considered as an

additional validation of the 3D RANS equation developed in CIAM and ability CFD code to accurately predict the efficiency of other high loaded single stage turbines.

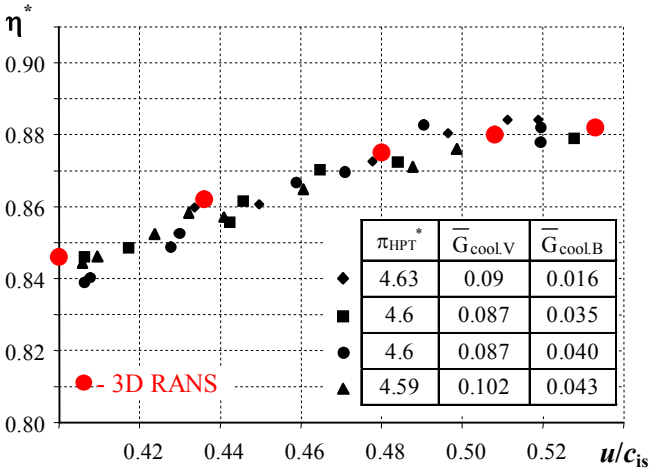

Fig. 2. HPT's efficiency versus speed coefficient u/c_{is}.

The Calculated results of the HPT were obtained using 3D RANS equations designed and developed in the CIAM [3] with a turbulence model of $(q-\omega)$ T.J. Coakley [4].

The dependence of the of the reactivity degree of the HPT upon a variation of the speed coefficient u/c_{is} with a different amount of the cooling air through the HPT's vanes and blades obtained at the regime with the stage pressure ratio of 4.6 are shown in Fig. 3. It can be noticed that within the investigated range of the cooling air through the HPT's vanes and blades the reactivity degree of 0.54 at the shroud of a flow part is almost constant.

The reactivity degree at the hub of the flow part increases significantly with an increase of the amount of cooling air through the HPT's blades. This is due to the fact that in this case there is an increase of the pressure of the air in the cooling system at the blades' inlet which contributes to an increase of its leakage to the axial gap of a flow part and, consequently, the losses in these sections.

Fig. 3 also shows that the level of reactivity degree in the HPT is relatively high and its averaged amount is 0.48-0.5, which is in good agreement with the calculated data.

In Fig. 4 the experimental variation HPT's efficiency are plotted versus the stage pressure ratio. This performance was obtained at the regimes with the speed coefficients 0.45, 0.5 and without cooling air through the HPT's vanes and blades. It is seen that HPT's efficiency increases very intense with increasing the stage pressure ratio.

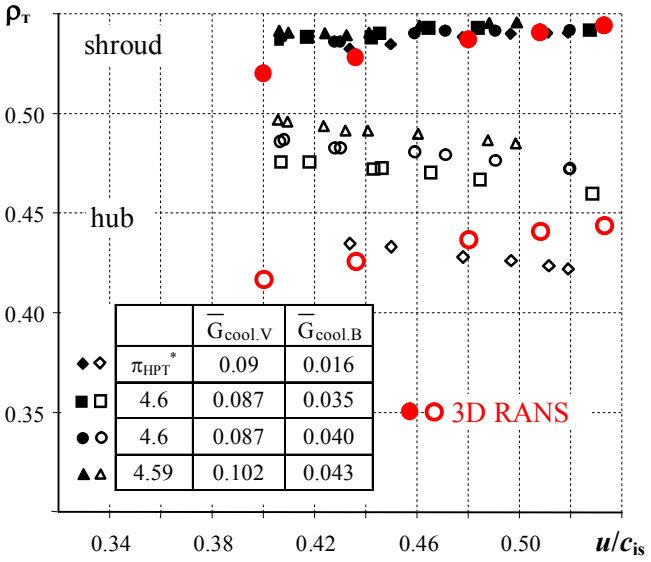

Fig. 3. The reactivity degree of the HPT versus the speed coefficient u/c_{is}.

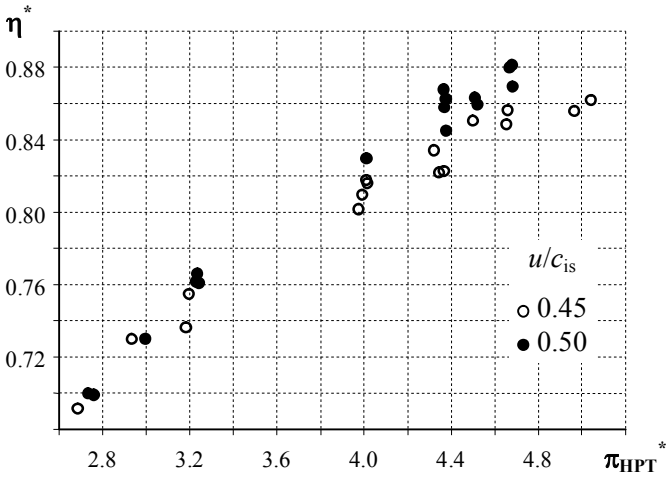

Fig. 4. The HPT's efficiency versus the stage pressure ratio at the regimes with the speed coefficient $u/c_{is} = 0.45$; 0.5 and $\overline{G}_{cool.V} = \overline{G}_{cool.B} = 0$.

5 Estimation of duct losses

As mentioned above, there is a significant flow swirl at the HPT's outlet at the design condition. In addition, the intense external shock waves can occur at the trailing edges of the blades. All this, combined with high level of the absolute velocity at the HPT's outlet can lead toward the high total pressure losses in the ID.

The calculated wave structure of the flow at the middle layer of the computational grid inside the HPT's blades and the ID for the

original (poor) version of the rotor blades is shown in Fig. 5 in position a). It is evident that external shock waves are spreading through the ID, that leads to a substantial increase in the total pressure losses there.

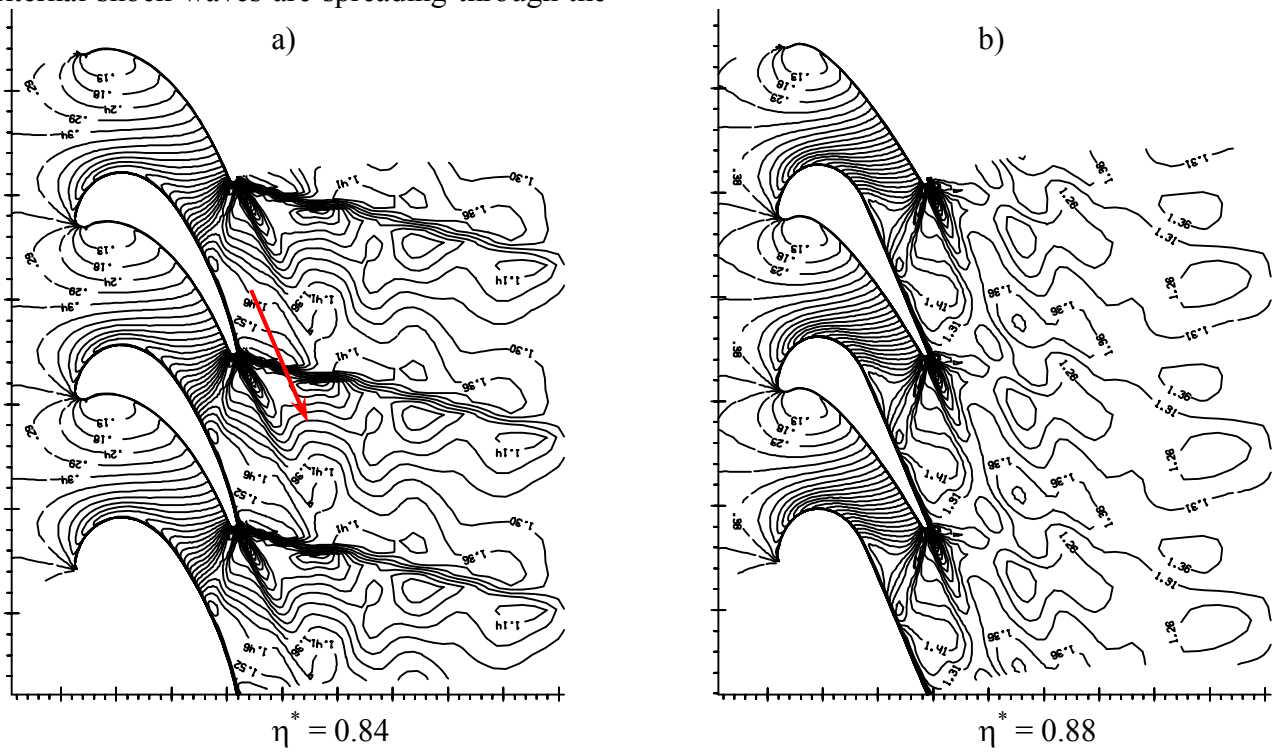

Fig. 5. Isolines of Mach number in the middle layer of the computational grid inside the HPT's blades and the ID: а) – original (poor) blades; б) – modified blades.

This is because the main mass flow during the passage through the ID crosses multiple shock waves, where the wave losses take place.

A similar pattern of the same ID but with the optimally designed rotor blades is shown in Fig. 5 in position b). In this case the external shock waves are absent at the blades' trailing edges and consequently inside the ID. Therefore the total pressure losses in the ID increase less intensively.

More clearly an increase of the total pressure losses along the length of the ID for the original blades and the modified blades (i.e., in the presence and absence of the external shock waves at the HPT's outlet) are shown in Fig. 6. In both cases, the calculations were carried out in the absence of the radial clearance of the rotor blades.

It could be noticed in Fig. 6 that the presence of shock waves at the HPT's outlet leads to the intense increase of the total pressure losses along the length of the ID. In the absence of shock waves the increase of the total pressure losses along the length of the ID occurs much more slowly.

In Fig. 7 the increase of the area averaged total pressure losses is shown along the relative length of the ID in the cases of presence and absence of the external shock waves at the HPT's outlet. As can be seen in Fig. 7, the total pressure losses in the ID in the presence of shock waves are almost four times more than in the absence of shock waves. In the case of the optimally modified HPT's blades the total pressure losses in the ID are approximately 0.025.

Consider the structure of the flow inside the ID in the absolute motion. The changing of the flow parameters in the middle layer of the computational grid for the relative time of the blades' passage is shown in Fig. 8 (where $\bar{\tau} = \tau/\tau_0$; τ_0 - the time for which the blade passes the distance equals to the blades' pitch; τ - a current time). The changing of the flow parameters in Fig. 8 are presented for the original blades at the relative length position along the ID of 0.05 and 0.5.

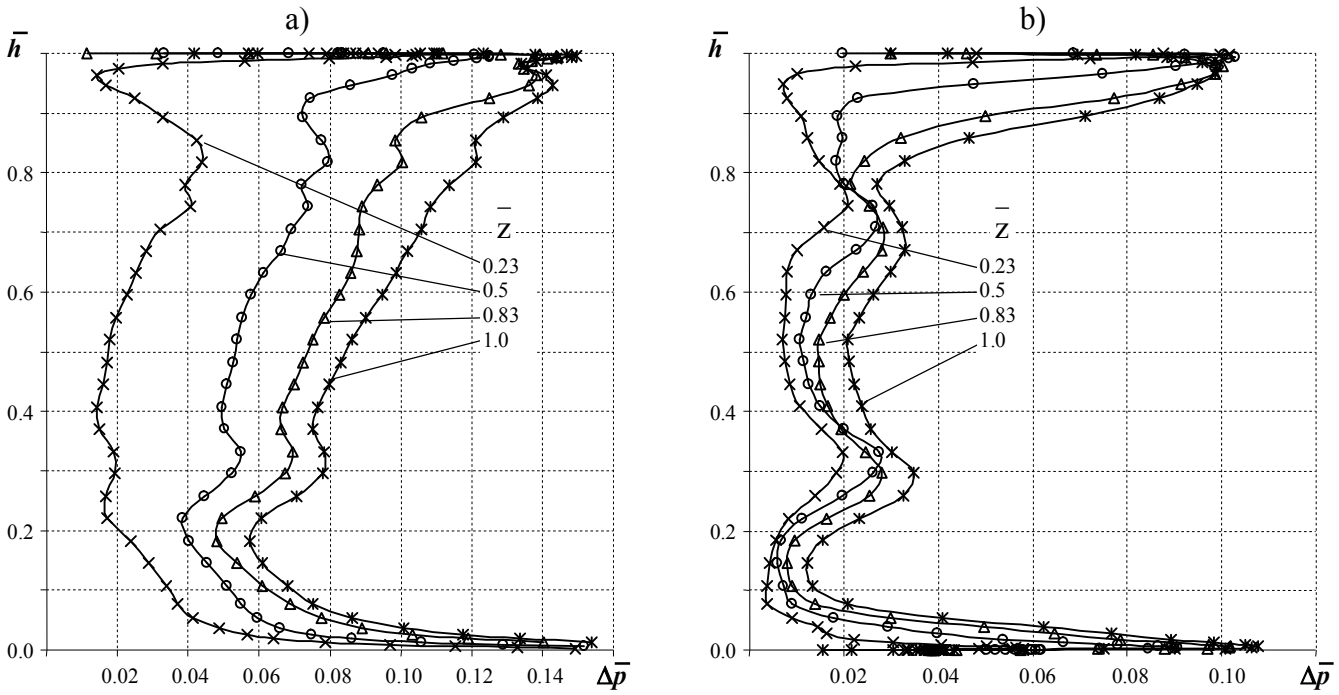

Fig. 6. The changes of the total pressure losses in the height of a flow part $\bar{h}$ at the different positions along the ID $\bar{z}$: a) – original (poor) blades; б) – modified blades.

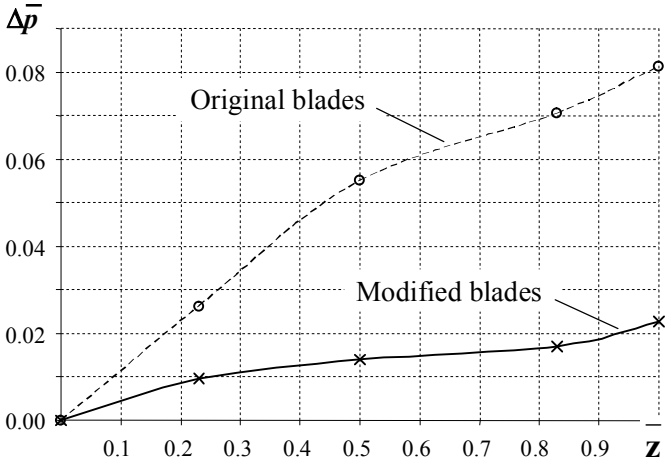

Fig. 7. The increase of the total pressure losses along the relative length of the ID.

Fig. 8 shows that the static pressure pulsations (and flow velocity pulsations) of the original blades at the ID's inlet reach extremely high values. As the distance from the blades the heterogeneity of the flow in the ID, of course, significantly decreases.

With the optimally modified blades the heterogeneity of the flow in the ID is significantly reduced.

The pulsations of static pressure and flow velocity in the absolute motion can be characterized by the ratio of maximum and minimum values p_{max}/p_{min} and c_{max}/c_{min} per one period blade's passage. These relations in the middle layer of the computational grid of the ID at the relative length position along the ID of 0.05 and 0.5 are shown in Table 2.

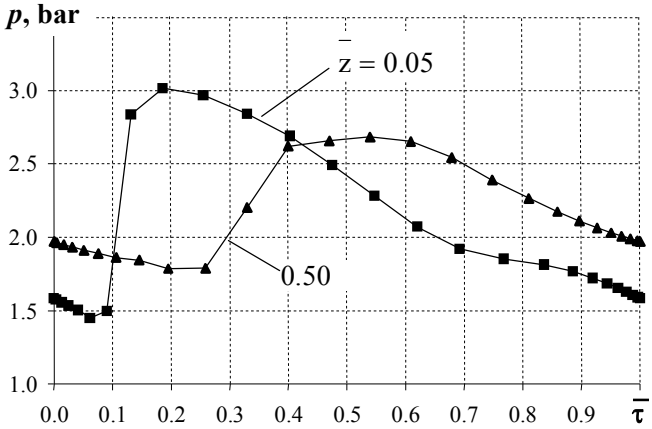

Fig. 8. The static pressure versus relative time of the blades' passage in the middle layer of the computational grid in the ID for the original blades (at the relative ID's length of $\bar{z}$ = 0.05; 0.50).

It can be seen in Table 2 that at the ID's inlet the ratio of the maximum and minimum static pressure per one period for the original blades is 2 (i.e., the static pressure at the same point of the channel changes in magnitude by 2 times with a frequency of about 16 000 Hz). The flow velocity

in the absolute movement per one period changes in magnitude by 1.6 times.

Table 2 The pulsations of the flow parameters in the ID

Blade	$\bar{z}$	p_{max}/p_{min}	c_{max}/c_{min}
Original	0.05	2.0	1.6
	0.50	1.5	1.2
Modified	0.05	1.2	1.12
	0.50	1.18	1.10

In the case of the modified blades (in the absence of external shock waves at the blades' trailing edges) the pulsations of the parameters in the absolute motion of the ID is much smaller.

6 Conclusion

- The calculated and experimental investigations of the high loaded single-stage cooled HPT were carried out in the CIAM. The experimental investigations were conducted within the module that included HPT + ID + first-stage nozzle block of the LPT + GV designed and manufactured in the Aviadvigatel. It was shown that at design point ($\pi_{HPT}^{*} \approx 4.6$; $u/c_{is} = 0.47 - 0.48$) at the model conditions with the high magnitude of the rotor tip clearance the efficiency of the HPT was 0.875. At the designed magnitude of the rotor tip clearance of 0.45 mm the increase of the efficiency could be about 0.015 and the HPT's efficiency at the model conditions could be 0.89.
- Under the engine operating conditions at the designed magnitude of the rotor tip clearance due to the high turbulence level at the HPT's inlet the decrease of the efficiency could be about 0.01 and the HPT's efficiency could be 0.88.
- The total pressure losses in the ID depend not only on its shape, but also on the flow parameters and the flow structure at the HPT's outlet. In the presence of external shock waves at the HPT's outlet the total pressure losses in the ID increase very intensely due to repeated passage of the flow through the multiple shock waves. In the absence of the external shock waves at the blades' trailing edges the total pressure losses in the ID located after high loaded HPT could be 0.015-0.025
- The modern methods of designing a turbine's unit (HPT + ID + LPT) for a turbofan engine shall be based on the 3D calculation of the entire module. This allows to consider more accurately the boundary conditions at the inlet of each element of a flow part of a turbine's unit.

References

[1] Wolf T, Janke E, Benton R, Kost F, Haselbach F, Gegg S. Design and tests of highly loaded single-stage high pressure turbine. *ASME paper GT2011-45342*, 2011.

[2] Marn A, Göttlich E, Pecnik R, Malzacher F, Schennach O, Pirker H. The influence of blade tip gap variation on the flow through an aggressive s-shape intermediate turbine duct downstream a transonic turbine stage – part I: Time-averaged results. *ASME paper GT2007-27405*, 2007.

[3] Krupa V, Ivanov M. Solution of Navier-Stokes Equations using high accuracy monotone schemes in Mathematical Models of Gas Turbine Engines and their Components. *AGARD Lecture Series TCP 02/LS 198*, pp 3-1 – 3-16, 1994.

[4] Coakley T. Turbulence modeling methods for compressible Navier-Stokes equations. *AIAA Paper*, №83-1693, p.13, 1983.

Copyright Statement